



DESY Summer School 2015 – Theory Group

π^2 -Resummation of N³LO Predictions for Gluon Fusion Higgs Production

Summer Student Report

Johannes Michel

18th September 2015



Supervisors: Frank Tackmann
Markus Ebert

Abstract

The hard function for gluon fusion Higgs production is extended to N³LO in an effective one-step matching scheme. Using renormalization group evolution, the convergence of its perturbative series is investigated for different choices of the hard scale μ_H . The prescription $\mu_H = -im_H$ of π^2 -resummation is found to be a natural choice, yielding the fastest convergence. Alternative matching schemes are compared to the one employed. Extending π^2 -resummation to most recent N³LO results for the total cross section, improved estimates for perturbative uncertainties are obtained. For the Drell-Yan process, π^2 -resummation of the hard function is observed to slightly improve its convergence.

Acknowledgments

I would like to express my gratitude to my supervisors Frank Tackmann and Markus Ebert for encouraging and extended discussions. I am indebted to Frank Tackmann in particular for the intriguing topic and to Markus Ebert for introducing me to the SCETlib framework. Yet, I can no longer thank them for enduring my silliest mistakes as they were already reimbursed for this in cookies. I would also like to thank Piotr Pietrulewicz for being our mountain guide on the steep learning curve of effective field theories and SCET. My thanks extend to DESY Hamburg for hosting a great summer student program and to group T for the hospitality during this summer.

Contents

1. Introduction	3
1.1. Effective field theories	4
1.2. Soft-collinear effective theory	5
2. Ingredients of the $gg \rightarrow H$ hard function at N³LO	8
2.1. The top matching coefficient	9
2.2. The SCET hard matching coefficient	10
2.3. Renormalization-group evolution and π^2 -resummation	11
3. π^2-Resummed results for the $gg \rightarrow H$ hard function	12
4. Comparison of matching schemes	15
4.1. Two-step matching	16
4.2. One-step matching with a finite top mass	17
5. π^2-Resummation of the $gg \rightarrow H$ inclusive cross section	18
5.1. Resummation scheme	18
5.2. Numerical results and uncertainties	20
6. Outlook on the N³LO Drell-Yan hard function	24
7. Conclusions	26
A. Anomalous dimensions	27
B. Generic fixed order expansion of matching coefficients	27
C. Further numerical results	29
References	31

1. Introduction

With the launch of Run II at the LHC, the properties of the newly discovered Higgs-like particle [1, 2] are bound to become ever more precisely determined in experiment. Eventually, the ball will be back in the court of the theorists: In the quest for new physics, they are challenged to state what the Standard Model actually *says* about the properties of the Higgs accessible to experiment. This is by far not an easy task. The means currently employed to study the innermost “hard” interactions at the heart of hadron collisions – perturbation theory – are notoriously plagued by the bad convergence of the perturbative series obtained, mostly due to large logarithms of scales that intrinsically arise in processes involving multiple scales.

The key approach to resolving this problem is *resummation*: Consider some observable X (e. g. a cross section), given by a perturbative series in the strong coupling constant α_s ,

$$X = 1 + \alpha_s (x + y_1) + \alpha_s^2 \left(\frac{x^2}{2} + xy_1 + y_2 \right) + \dots$$

Now assume that some term x is known to appear in a fixed pattern at *every* order in perturbation theory – and also known to spoil the convergence of X . Resummation offers a remedy, by noting that X is nothing but

$$X = e^{\alpha_s x + \dots} Y, \quad Y = 1 + \alpha_s y_1 + \alpha_s^2 y_2 + \dots,$$

and Y may now be a series converging very neatly. In realistic examples, however, identifying the *pattern* becomes the major obstacle. As has been observed earlier [3], the “culprit” x in our case of gluon fusion Higgs production are logarithms $4C_A \ln^2(-im_H/\mu) \approx C_A \pi^2$, where $\mu \approx m_H$ is the renormalization scale. In order to correctly extract the perpetrating terms, effective field theories come into play: They identify parts of the interaction as operators that possess an explicit dependence on μ , something the renormalized Standard Model no longer contains traces of. What seems like a step backwards, can be turned into a virtue: By solving the renormalization-group (RG) equations of the effective operators in closed form,¹ the large logarithms can be evaluated at a more convenient scale (say, $\mu_H = -im_H$) and only afterwards evolved back to the “target” scale μ by the RG flow; the latter corresponds to $\exp(\alpha_s x + \dots)$ in the above example. From the aforementioned terms $\propto \pi^2$, dominant among the ones resummed, this resummation method has come to be known as “ π^2 -resummation” [4].

The aim of this analysis will be to apply π^2 -resummation to the most recent N³LO results in perturbative QCD for the total $gg \rightarrow H$ cross section [5]. The report is structured as follows: Some general remarks are made on effective field theories in section 1.1 and soft-collinear effective theory as a particularly important example

¹Or, rather, of the “matching coefficients” that relate them to the interaction terms of the full model.

in section 1.2. The ingredients needed for the later calculations are presented in section 2. Also given there are references to the more recent theoretical computations that allow for extending the approach of [3] to N³LO in the first place. We compare our matching scheme to the schemes of [6] and [7] in section 4 and proceed to present our results for the total cross section in section 5. In section 6, π^2 -resummation for the Drell-Yan process at N³LO is briefly discussed, extending again considerations by the authors of [3] at NNLO. We conclude in section 7.

1.1. Effective field theories

Top-down effective field theories (EFTs) are centered around the idea of removing heavy degrees of a freedom from a full model to simplify it.² To this end, the full Lagrangian is expanded in terms of a suitable smallness parameter λ ,

$$\mathcal{L}_{\text{full}} = \sum_n \mathcal{L}_{\text{eff}}^{(n)}, \quad \mathcal{L}_{\text{eff}}^{(n)} \propto \lambda^n. \quad (1.1)$$

Often, the expansion will only include the leading term and neglect even the first power-suppressed term $\mathcal{O}(\lambda)$. A famous example is Fermi theory: Here, the smallness parameter is the inverse $\lambda = 1/m_{W,Z}$ of the vector boson masses.³ The leading interaction term $\mathcal{L}_{\text{int}}^{(0)}$ reproduces the well-known four-point interaction of fermions, as can be expected from approximating $s - m_W^2 \approx -m_W^2$ in the W -propagator of the tree-level diagram in fig. 1. More formally, the vector boson degrees of freedom can be integrated out explicitly in the functional integral or eliminated from the Lagrangian directly by means of their equation of motion.

The complexity of the problem increases when loops are admitted: Since it contains an interaction Hamiltonian having mass dimension six, Fermi theory will never be renormalizable in the traditional sense of introducing a finite set of regulator-dependent parameters, thereby canceling all divergencies to all orders. (This just comes to illustrate that the effective theory can not be trusted in the UV-limit. The same will be the case in the examples of EFTs considered later on.) However, the effective operator $\mathcal{L}_{\text{int}}^{(0)}$ may still be renormalized by a finite set of parameters Z_{eff} such that divergencies cancel *up to a given order* in perturbation theory. As usual, the respective renormalization factor will cancel the dependence of the bare operator on any regulators; yet, the renormalized operator inherits a dependence on the renormalization scale μ from its renormalization factor.

Having renormalized the full model to all orders and the EFT as desired, we are then enabled to *match* the two: By computing the same amplitudes in both theories and requiring that they are equal, we can determine the missing factor C between

²This short introduction is entirely owed to the lecture notes by Stewart [8].

³For a dimensionful parameter λ , “smallness” and omitting the power-suppressed terms are only justified *a posteriori* when computing amplitudes at center of mass energies $\sqrt{s} \ll m_{W,Z}$. In later examples, λ will be dimensionless.

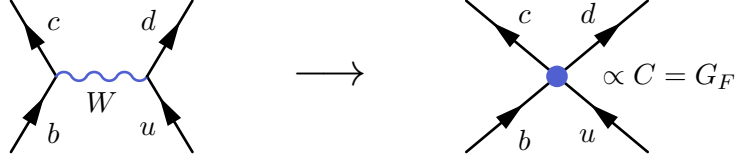


Figure 1: The matching necessary between the Standard Model and Fermi theory, at the example of b -decay (no particular kinematics implied). Note that the matching coefficient(s) C will receive corrections e.g. from QCD loop diagrams in both models at higher orders.

the full and the effective operator, called “Wilson” or “matching coefficient”. This will only at tree-level be a trivial constant, as in the case of the diagrams in fig. 1: At higher orders, the Wilson coefficient will rather be an involved perturbative series in couplings giving rise to loops, usually α_s of QCD. It is of particular importance to our application that C will in fact be $C(\mu)$, canceling the μ -dependence of the effective field theory matrix element to yield the μ -independent full theory amplitude. If C satisfies an RG equation

$$\mu \frac{d}{d\mu} C(\mu) = \gamma_C(\mu) C(\mu) ,$$

the solution in closed form reads

$$C(\mu) = C(\mu_H) U_C(\mu_H, \mu) , \quad U_C = \exp \left[\int_{\mu_H}^{\mu} \frac{d\mu'}{\mu'} \gamma_C(\mu') \right] .$$

As hinted at in the introduction, this will enable us to evaluate $C(\mu_H)$ at a “natural” scale μ_H leading to an improved convergence. Afterwards, U will be employed to bridge the gap to the original scale μ , resumming as an exponential the offending terms in the perturbative series of $C(\mu)$.

1.2. Soft-collinear effective theory

Soft-collinear effective theory (SCET) is a rather peculiar EFT, as it does not involve integrating out an entire particle: Rather, the degrees of freedom present in QCD – gauge and quark fields – are split into sets of modes, according to their momentum components in different directions.⁴ While originally developed to study the decay of heavy into light quarks [10], SCET soon came to be used for hadron-hadron collisions and jet physics, too. In all of these applications, light cone coordinates are introduced: Consider two light-like unit vectors

$$n^2 = 0 , \quad \bar{n}^2 = 0 , \quad n \cdot \bar{n} = 2 .$$

In hadron-hadron collisions, these may be aligned with the directions of the incoming hadrons; for a given number of final state jets, we may even choose one set of light-cone coordinates n_i, \bar{n}_i aligned along each jet direction. Any momentum p can then

⁴This section again draws on the very informative lecture notes by Stewart [9].

uniquely be decomposed into

$$p = (p^+, p^-, \vec{p}_\perp) ,$$

where $p^+ = n \cdot p$, $p^- = \bar{n} \cdot p$ and \vec{p}_\perp is the remaining Euclidean momentum. All modes in the theory can now be characterized by the scaling of their components: In the example of a final state jet, we could define a smallness parameter $\lambda = \Delta/Q$, where Q is the energy of one of the collimated particles in the jet and $\Delta \ll Q$ measures the slight transverse deviation of its momentum from the jet direction. In short, this “collinear” scaling law reads

$$p_{\text{collinear}} \propto Q(\lambda^2, 1, \lambda) .$$

Note that λ is a *generic* parameter that can not be given an exact definition – in particular, the meaning given to it will depend on the process that SCET is applied to. On the other hand, modes with a homogeneous scaling in all components are called (ultra-)soft,⁵

$$p_{\text{soft}} \propto Q(\lambda, \lambda, \lambda) , \quad p_{\text{ultrasoft}} \propto Q(\lambda^2, \lambda^2, \lambda^2) .$$

Finally, modes with an invariant mass (read: large off-shellness) $\propto Q^2$ are deemed “hard” – we can not expect to observe them in a final state. It is precisely these modes with large virtuality in intermediate states that fall prey to the process of integrating out, just as the vector bosons of electroweak theory did not make it into Fermi theory. The remaining degrees of freedom in SCET then are collinear and (ultra-)soft quark and gluon fields, respectively; to preserve gauge invariance of these remaining degrees of freedom order by order in λ , the fermion fields are dressed with Wilson lines.

To illustrate the concepts of SCET (and do some conceptional groundwork for the main part of the analysis), we outline the steps of one example of a matching calculation, skipping any derivation of the SCET-Lagrangian and all Feynman rules. Consider the Drell-Yan process in hadron collisions,⁶ having at its core the hard interaction $q\bar{q} \rightarrow Z/\gamma^* \rightarrow \ell^+\ell^-$. The tree-level matching between full QCD and SCET is trivial: In both theories, the relevant $q\bar{q} \rightarrow Z/\gamma^*$ part of the interaction simply is a fermion chain with some vertex Dirac structure Γ in between. Of course, finding the matching coefficient C relating the two operators at NLO is more involved (fig. 2, from left to right): In full QCD, a diagram containing an additional gluon line between the external quark enters; in SCET, two discernible contributions arise. In one case, the initial state quarks (collinear to either n or \bar{n}) exchange an ultrasoft gluon before entering the electroweak interaction. The second diagram originates

⁵This seemingly subtle distinction carries through all the way into theories constructed on the basis of one of the two cases: Ultrasoft modes (SCET I) have an invariant mass squared scaling as $\propto \lambda^4$ and therefore can be distinguished from collinear modes $\propto \lambda^2$ by their invariant mass in mass-independent regularization. Soft modes (SCET II), however, also possess an invariant mass scaling as λ^2 and can become collinear after a simple boost, making them exponentially harder to disentangle.

⁶In [9], the equivalent example of $e^+e^- \rightarrow 2$ jets is presented in far more detail.

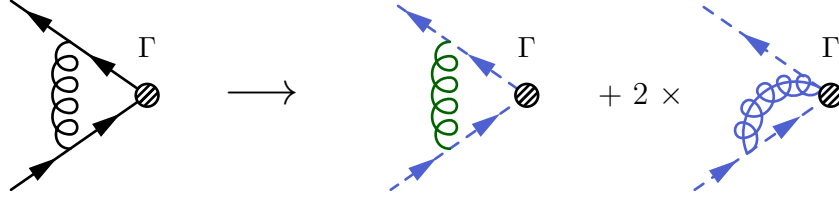


Figure 2: Diagrams required in the NLO matching for the Drell-Yan process. The QCD diagram on the l. h. s. upon renormalization essentially gives the quark form factor; in SCET, the exchange of an ultrasoft gluon (in green) and the contraction of one collinear Wilson line with the respective other collinear quark (all depicted in blue) have to be considered. See the text for more detail.

from the $\mathcal{O}(\alpha_s)$ expansion of the collinear Wilson lines: Since the emission of a collinear gluon in the opposite direction pushes the emitting quark far off shell, the gluon in SCET can be considered as emitted from the electroweak vertex directly; interchanging “emitter” and “receiver” yields an identical contribution from the mirror diagram.

When actually evaluating the diagrams, a slight twist comes about, depending on the choice of regulators. In a first scenario, we may choose some off-shellness p^2 of the outer quark legs to regulate IR- and $\varepsilon = (D - 4)/2$ to regulate UV-divergencies. As is well known, the QCD diagram – being essentially the quark form factor – will still be IR-divergent after wave function renormalization cancels the pole in ε . SCET reproduces precisely the same divergencies in p^2 , as expected – it contains the same collinear and soft modes that lead to the IR-divergency in QCD. The matching coefficient C will therefore be IR-finite. However, the SCET amplitude will contain additional ε -poles. In the spirit of section 1.1, these are removed by a multiplicative renormalization term Z_C for the SCET operator, making C also finite in ε , but dependent on the renormalization scale μ .

In a second case, we may instead opt for pure dimensional regularization, with an obvious computational advantage: Both SCET diagrams vanish, leaving behind only one $\mathcal{O}(\alpha_s)$ -contribution from the SCET wave function renormalization. Yet, the IR-divergency of the QCD diagram is now encoded in ε -poles: To cancel these and obtain a finite matching coefficient C , the same multiplicative renormalization by Z_C as above will have to be applied. Note that this means that in $\overline{\text{MS}}$, we are forced to *reinterpret* IR-divergencies of QCD as UV-divergencies of SCET (otherwise we would not be able to remove them by renormalization), with powerful implications: The anomalous dimension in the RG evolution of C and the finite terms in C may be predicted entirely from calculations in pure QCD, either from the IR-poles or the IR-finite terms. By exploiting these relations, the authors of [11] are able to convert their dedicated N³LO computations of form factors in QCD into N³LO results for SCET matching coefficients – results that will repeatedly be used in this analysis.

2. Ingredients of the $gg \rightarrow H$ hard function at $N^3\text{LO}$

In the following section, we present the ingredients needed to compute the hard function for gluon fusion Higgs production at $N^3\text{LO}$. The hard function encodes information on virtual contributions to $gg \rightarrow H$ which are “hard” in the sense that they arise from quantum fluctuations in modes $\gtrsim m_H$. For the purpose of this analysis, we consider these quantum fluctuations to have two distinct origins: One is the virtual t -quark running in the famous “top triangle” loop that only allows for gluon-gluon-Higgs interaction in the first place, also including – at the order in perturbative QCD we require – the exchange of colored particles *within* the loop and between the top and the incoming gluons. The characteristic scale of these dynamics is the top mass m_t . The second origin of virtual corrections is the exchange of hard ($\approx m_H$) color-carrying modes between the incoming gluons only. Here, the implicit assumption is that the top quark is sufficiently heavy to justify the separation of scales: We formally require $m_t \gg m_H$.

The distinction between two different hard contributions is reflected in the formal makeup of the hard function we employ. As in ref. [7], we define the hard function by means of an effective field theory matching coefficient C_{ggH} at a renormalization scale μ ,

$$H(q^2; \mu) = |C_{ggH}(q^2; \mu)|^2 \quad (2.1)$$

where the invariant mass q^2 of the Higgs boson (and thus of the WW or photon pair in viable final states) is always assumed to be $q^2 = m_H^2$ for an on shell Higgs in the narrow width approximation. Conforming again with [7], the Wilson coefficient C_{ggH} matches the full Standard Model interactions onto an effective Hamiltonian for the coupling between the Higgs field H and the collinear gluon field. The latter is the SCET degree of freedom relevant to our analysis after all of the aforementioned hard modes have been integrated out. However, in staying true to our assumption of two *distinct* types of hard fluctuations, the hard modes are integrated out in two steps, as in the framework of [6]: In a first step, the full model with $n_f = 6$ quark flavors is matched onto a $n_f = 5$ model including an effective ggH -vertex. The Wilson coefficient C_t relating the two interaction terms is introduced in section 2.1, while fig. 3 illustrates the matching step. Note that we do not include the overall factor of α_s from the gluon-quark vertices of the “top-triangle” into C_t . In a second step performed in section 2.2, we match the remaining interaction term onto the effective Hamiltonian in SCET via another Wilson coefficient C_H . Both sections essentially extend the NNLO results of [6] to the next order, either relying on the renormalization-group properties of C_t or on recent $N^3\text{LO}$ results for C_H from the literature. The total matching coefficient then factorizes into

$$C_{ggH}(m_H^2, m_t^2; \mu) = \alpha_s(\mu) C_t(m_t^2; \mu) C_H(m_H^2; \mu) . \quad (2.2)$$

Its RG evolution is discussed in section 2.3; comments on the choice of evaluating *both* Wilson coefficients in (2.2) at the same scale μ will be deferred to section 4.

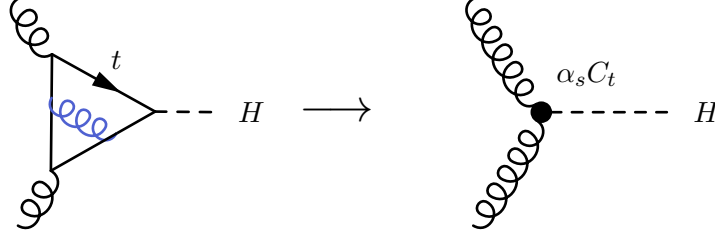


Figure 3: The “top triangle” loop diagram and the effective theory diagram it is matched on to compute C_t . A two-loop contribution at NLO in perturbative QCD is shown in blue.

2.1. The top matching coefficient

Following the path of [6], the Wilson coefficient C_t of the first step discussed above is obtained by matching the $n_f = 6$ Standard Model onto an effective interaction Hamiltonian

$$\mathcal{H}_{\text{eff}}^{n_f=5} = -C_t(m_t^2; \mu) \frac{H}{v} \frac{\alpha_s(\mu)}{12\pi} G_{\mu\nu,a} G_a^{\mu\nu} . \quad (2.3)$$

Here, $v = (\sqrt{2}G_F)^{-1/2} \approx 246 \text{ GeV}$ is the Higgs vacuum expectation value, m_t is the top pole mass and $G_{\mu\nu,a}$ still is the full QCD gluon field strength. Since the renormalized Standard Model interaction term on an imagined “left hand side” of (2.3) must be independent of the renormalization scale μ , C_t must precisely cancel the μ -dependence of the mass dimension five operator to its right (including the overall factor of α_s). The resulting renormalization-group equation reads [6]

$$\mu \frac{d}{d\mu} C_t = \gamma^t C_t , \quad \gamma^t(\alpha_s) = \alpha_s^2 \frac{d}{d\alpha_s} \frac{\beta(\alpha_s)}{\alpha_s} \quad (2.4)$$

when expressed in terms of the $n_f = 5$ running coupling and its β -function.⁷ Casting the anomalous dimension γ^t in the form (A.2) leaves

$$\gamma^t = \sum_{n=0}^{\infty} \gamma_n^t \left(\frac{\alpha_s}{4\pi} \right)^{n+1} , \quad \gamma_n^t = -2n \cdot \beta_n . \quad (2.5)$$

Setting out from (2.4), the fixed order expansion of C_t can readily be predicted to a great extent: In appendix B, this is done for a more generic Wilson coefficient. Noting that the anomalous dimension of (2.4) contains no direct logarithmic dependence on the scale, the top matching coefficient at hand is one of the easiest applications of

⁷Unless stated otherwise, the strong coupling constant always undergoes three-loop running in this analysis, assuming $n_f = 5$ quark flavors. Wherever numerical values are displayed, the boundary condition $\alpha_s(m_Z) = 0.117$ is employed, consistent with the choice of [5].

the general N³LO expansion in (B.5):

$$\begin{aligned}
 C_t(m_t^2; \mu) = & 1 + \frac{\alpha_s(\mu)}{4\pi} d_t^{(1)} + \left(\frac{\alpha_s(\mu)}{4\pi} \right)^2 \left[L_t \left(\beta_1 - \beta_0 d_t^{(1)} \right) + d_t^{(2)} \right] \\
 & + \left(\frac{\alpha_s(\mu)}{4\pi} \right)^3 \left[L_t^2 \left(\beta_0^2 d_t^{(1)} - \beta_0 \beta_1 \right) + 2L_t \left(\beta_2 - \beta_0 d_t^{(2)} \right) + d_t^{(3)} \right] ,
 \end{aligned} \tag{2.6}$$

where $L_t := \ln(m_t^2/\mu^2)$ and the constant terms at $L_t = 0$ through NNLO can be read off from the results in [6]:

$$\begin{aligned}
 d_t^{(1)} &= 5C_A - 3C_F , \\
 d_t^{(2)} &= \frac{27}{2}C_F^2 - \frac{100}{3}C_A C_F + \frac{1063}{36}C_A^2 - \frac{4}{3}C_F T_F \\
 &\quad - \frac{5}{6}C_A T_F - 5C_F T_F n_f - \frac{47}{9}C_A T_F n_f
 \end{aligned}$$

The only piece lacking in (2.6) therefore is the constant term $d_t^{(3)}$ at N³LO. Unfortunately, results for the N³LO contribution to C_t are currently only available in terms of the $\overline{\text{MS}}$ top mass and the $n_f = 6$ running coupling [12, 13]. If the numerical value of the constant terms in the results cited (accounting for the decoupling relations in the same references) can be trusted as an indicator for the size of $d_t^{(3)}$, a numerical estimate gives $|d_t^{(3)}| \approx 300$. This would turn out to be small when compared to the constant contributions of C_H , $d_H^{(3)} \approx -4065.52$ at the same order. It is also small compared to the scale-dependent N³LO terms $\propto L, L^2$ in (2.6) when μ is set to an imaginary scale. We set $d_t^{(3)} = 0$ in the following but suggest correctly converting the pole mass results for future investigations at N³LO.

2.2. The SCET hard matching coefficient

In a second step, we match the effective theory with $n_f = 5$ from the preceding section onto SCET by means of another matching coefficient C_H . Following the notation of [7], the required matching reads

$$-G_{\mu\nu,a} G_a^{\mu\nu} = C_H(q^2; \mu) q^2 g_{\mu\nu} \mathcal{B}_\perp^{\mu,c} \mathcal{B}_\perp^{\nu,c} . \tag{2.7}$$

In the above, \mathcal{B}^c is the collinear gluon field, being the sole relevant SCET degree of freedom for our purposes, assuming that all collinear and soft real radiation has been factorized into the so-called beam and soft functions [7]. The hard matching coefficient C_H satisfies the RG equation [6]

$$\mu \frac{d}{d\mu} C_H = \left[\Gamma^A(\alpha_s) \ln \frac{-m_H^2 - i0}{\mu^2} + \gamma^H \right] C_H , \tag{2.8}$$

where γ^H is called the “non-cusp” and Γ^A the “cusp” anomalous dimension. Both have perturbative expansions of the form (A.2) known analytically up to three-loop.⁸

⁸Sources cited for the coefficients are compiled in a table in appendix A.

While the former is process-dependent, the latter has so far been observed to be universal for the hard matching coefficients of color-singlet production up to an overall color factor (“Casimir scaling”).

As hinted at in the introduction, all necessary information about C_H can be retrieved from calculations of the gluon form factor in pure QCD: The fixed order expansion of C_H is just the IR-finite part of the renormalized gluon form factor, while the latter’s remaining IR-divergencies return the anomalous dimensions entering the RG evolution (2.8) of C_H .⁹ For the following computations, we rely on the full fixed order expansion of C_H obtained by the authors of [11]. However, we restrict ourselves to implementing their constants terms at $L = 0$ and for the remainder of the polynomial expressions $C_H^{(n)}(L)$ in

$$C_H(m_H^2; \mu) = 1 + \sum_{n=1}^{\infty} \left(\frac{\alpha_s(\mu)}{4\pi} \right)^n C_H^{(n)}(L) , \quad L := \ln \frac{-m_H^2 - i0}{\mu^2} \quad (2.9)$$

make recourse to the general expansion in terms of the anomalous dimensions derived in appendix B. Here, a twofold advantage of the very generic expression (B.5) becomes apparent: On a more practical side, it greatly reduces the effort of implementing a N³LO Wilson coefficient in numerical computations. Conceptionally, it makes explicit the connection between coefficients in front of potentially large powers of logarithms L^m and anomalous dimensions in the very same RGE that is employed to resum them. As an example, Γ^A controls “Sudakov logarithms” in a rather obvious sense: Wherever a term $\alpha_s^n L^m$, $m > n$ arises in the full expansion (2.9), it receives a prefactor of $(\Gamma_0^A)^{m-n}$.

2.3. Renormalization-group evolution and π^2 -resummation

The relation $\mu(d\alpha_s/d\mu) = \beta(\alpha_s)$ and the RG equations (2.4), (2.8) can be combined into

$$\mu \frac{d}{d\mu} C_{ggH} = [\Gamma^A \cdot L + \gamma^{ggH}] C_{ggH} , \quad \gamma^{ggH} = \gamma^H + \gamma^t + \frac{\beta}{\alpha_s} . \quad (2.10)$$

As is well established, the above RG equation is solved by

$$C_{ggH}(\mu) = \exp [L(\mu_H) \cdot \eta_{\Gamma,A}(\mu_H, \mu) - 2K_{\Gamma,A}(\mu_H, \mu) + K_{\gamma,ggH}(\mu_H, \mu)] \times C_{ggH}(\mu_H) , \quad (2.11)$$

⁹On a more subtle note, C_H at higher orders also receives cross-terms between the subleading terms $\mathcal{O}(\varepsilon^n)$, $n > 0$ in the form factors and the ε -poles contained in the multiplicative renormalization factor. It is therefore crucial to compute the form factors to a sufficiently high order in ε .

where the functions η_Γ , K_Γ and K_γ are defined as¹⁰

$$\begin{aligned}\eta_\Gamma &= \int_{\mu_H}^{\mu} \frac{d\mu'}{\mu'} \Gamma(\alpha_s(\mu')) , & K_\Gamma &= \int_{\mu_H}^{\mu} \frac{d\mu'}{\mu'} \Gamma(\alpha_s(\mu')) \ln\left(\frac{\mu'}{\mu_H}\right) , \\ K_\gamma &= \int_{\mu_H}^{\mu} \frac{d\mu'}{\mu'} \gamma(\alpha_s(\mu')) .\end{aligned}\tag{2.12}$$

The pivotal point of π^2 -resummation now is to analytically continue the r.h.s. of (2.11) as a function of μ_H into the complex plane, noting that the l.h.s. remains unchanged, and to evaluate it at the scale μ_H yielding the best perturbative convergence of $C_{ggH}(\mu_H)$. This also requires us to analytically continue the running coupling into the complex plane [6]. For all practical considerations, we turn to the hard function (2.1): After evaluating all the factors of C_{ggH} at μ_H , squaring them separately and reexpanding the product in $\alpha_s(\mu_H)$, the resulting hard function can be RG evolved as

$$H(m_H^2, m_t^2; \mu) = H(m_H^2, m_t^2; \mu_H) U_H(\mu_H, \mu) ,\tag{2.13}$$

where U_H is the absolute value squared of the exponential in (2.11). Figure 6 (a) shows the procedure and the scales involved.

3. π^2 -Resummed results for the $gg \rightarrow H$ hard function

After the previous section has set the stage, we are enabled to investigate the behaviour of the RG evolved hard function for different choices of the hard scale μ_H and the real-valued “target” scale μ . Traditionally, $\mu_H = \mu$ is set and μ is chosen such as to partially minimize higher order corrections. We generalize this approach by adding an additional phase $\varphi \in [0, 3\pi/4]$ to μ_H :

$$\mu_H = \mu e^{-i\varphi}\tag{3.1}$$

Note that we still adhere to $|\mu_H| = \mu$: While our framework would easily allow for simultaneous variation of $|\mu_H|$ and φ , we restrict ourselves to varying the latter to isolate its effects on the perturbative convergence. The relevant values of μ are $m_H/2$ and m_H , the same that the authors of [5] focus on.

Figure 4 displays our numerical results for the RG evolved $gg \rightarrow H$ hard function $H_{\text{res}} := H(\mu_H) U_H(\mu_H, \mu)$. Here – as for all following numerical output – we set $m_t = 173.5$ GeV and $m_H = 125$ GeV. We vary both the phase φ and the fixed order at which the expansion of $H(\mu_H)$ is truncated. Regardless of the fixed order chosen,

¹⁰For a consistent expansion, the expressions are rewritten as integrals of the running coupling via $d\mu/\mu = d\alpha_s/\beta(\alpha_s)$. (The logarithm in K_Γ is re-expressed as an integral for this purpose.) Explicit expressions for η_Γ , K_Γ and K_γ through NNLL can be found in appendix B.3 of [7]. These were also implemented in the existing framework of `SCETlib` [14] used for our numerical computations.

U_H is always evaluated at NNLL precision. The main reason for this choice is our stated objective to study the perturbative *convergence* of the hard function. This is obviously facilitated by having all fixed order results undergo RG evolution by the same factor. While NNLL precision even becomes redundant in the LO and NLO case, an evolution factor through N³LL would be desirable for a consistent truncation in the N³LO case. Yet, evaluation of U_H through N³LL would require the four-loop coefficient Γ_3^A of the cusp anomalous dimension, unknown to date. We remark that the NNLL correction already is small but have to leave resummation at N³LL to future work.

We would like to point out three main observations on the results in fig. 4. First and foremost, the convergence of the hard function is indeed greatly improved for $\varphi \approx \pi/2$ in comparison to fixed order results at $\varphi = 0$ (left edge of the plots) as well as to $\varphi \approx 3\pi/4$ (right edge): The improvement is remarkable for the NLO result, almost yielding the N³LO result in the case of $\mu = m_H/2$ in fig. 4 (a) and giving a far better approximation at $\mu = m_H$ in (b). Similarly, the NNLO correction is greatly reduced by resummation from roughly 15 % to a relative contribution of ≤ 4 %. The reduction in the N³LO correction is particularly marked for the case $\mu = m_H$: Turning to the detail plots in the bottom row, we can read off a relative contribution of ≈ 0.3 %. To further illustrate the improved convergence, we give numerical values for the normalized fixed order expansions at $\varphi = 0$ and $\varphi = \pi/2$ for the example of $\mu = m_H$:

$$\begin{aligned} H/H_{\text{LO}}|_{\mu_H=m_H} &= 1 + 0.8099 + 0.3558 + 0.0992 , \\ H/H_{\text{LO}}|_{\mu_H=-im_H} &= 1 + 0.2695 + 0.0417 - 0.0033 \end{aligned} \quad (3.2)$$

The contributions at NⁿLO are roughly cut by a factor of $1/3^n$, making the perturbative series at $\mu_H = -im_H$ the one converging the most steadily among the scales considered here. These large improvements are in fact due to $\mu_H = -im_H$ simultaneously minimizing the NLO *through* N³LO corrections to the hard matching coefficient C_H . This should not be surprising as C_H contains Sudakov logarithms L^{2n} at all orders NⁿLO that we expect to be dominant and forcibly eliminate $L \rightarrow 0$ as $\varphi \rightarrow \pi/2$. When C_H is squared, its perturbative coefficients $C_H^{(n)}$ mix and contribute to H at different orders. Therefore, a “compromise” for minimizing the higher order corrections to C_H will yield an optimized convergence of H , as in the case of $\mu_H = -im_H$. For completeness, we give numerical results for C_H in a manner analogous to fig. 4 in appendix C, fig. 12.

Second, we observe that the newly available N³LO results are remarkably stable under variations of the phase,¹¹ with maximum deviations of ≈ 1 %. This indicates that at N³LO, the hard function is already very close to satisfying the all-orders expression (2.13) we employ to resum it. However, it also emphasizes the need to include the N³LO results, as lower orders would lead to larger uncertainties from variation of φ . Lastly, some insight can be gained from the behavior of the LO

¹¹The remaining discrepancy between the absolute values at $\mu = m_H/2$ and m_H is due to RG evolution *along* the real axis.

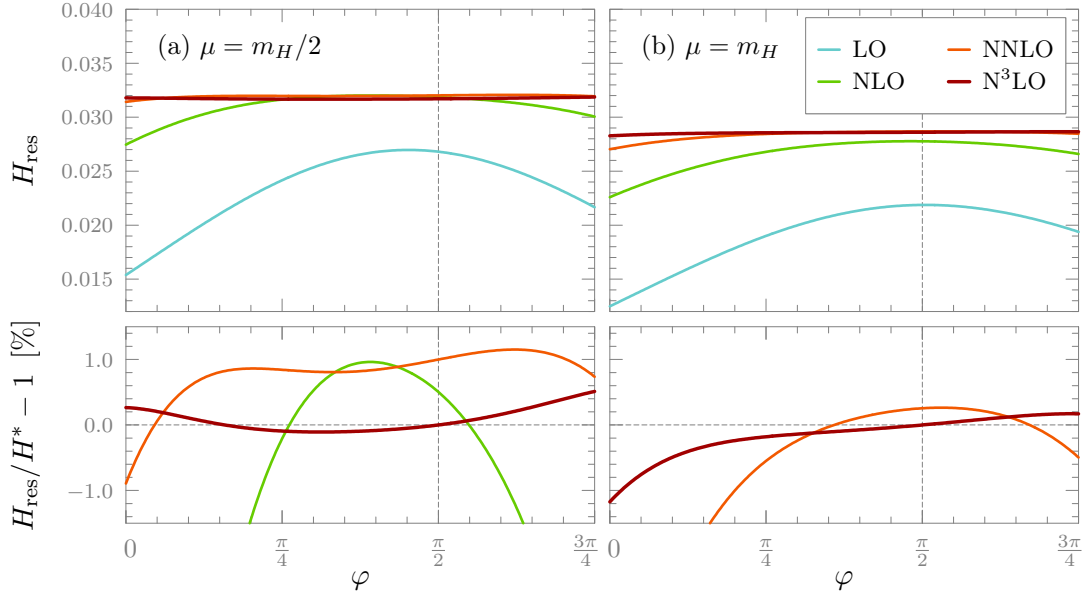


Figure 4: Numerical results for the RG evolved hard function $H_{\text{res}} = H(\mu_H) U_H(\mu_H, \mu)$ as a function of φ , $\mu_H = \mu e^{-i\varphi}$, where (a) $\mu = m_H/2$ on the left and (b) $\mu = m_H$ on the right. The fixed order expansion of $H(\mu_H)$ is truncated at the order indicated by the colors, with darker colors corresponding to higher orders. The evolution factor U_H is evaluated at NNLL precision throughout. In the top row, absolute values are displayed. The bottom row (detail) shows the relative deviation from the $N^3\text{LO}$ value H^* at $\varphi = \pi/2$ for each value of μ respectively.

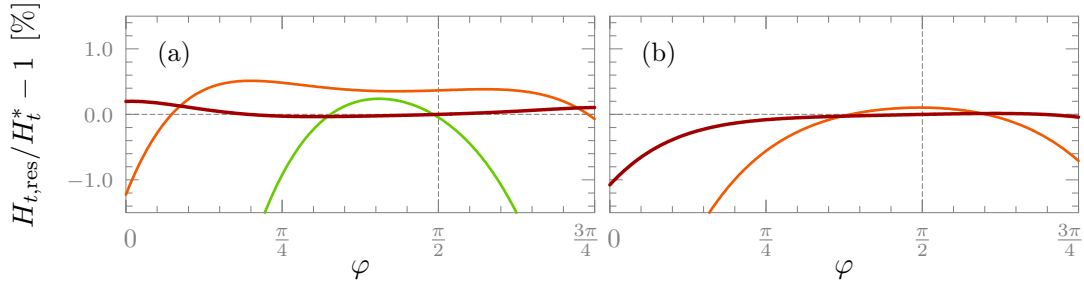


Figure 5: The RG evolved hard function $H_{t,\text{res}} = H_t(\mu_H) U_H(\mu_H, \mu)$, including independent running of C_t and internal resummation by U_t . The specifics of the figure are identical to the detail plots in the bottom row of fig. 4 above: Colors again indicate fixed orders; we vary the phase φ of μ_H , while $\mu_t = m_t$ is fixed; given here is the relative deviation from the $N^3\text{LO}$ value H_t^* at $\varphi = \pi/2$. The value of μ is (a) $m_H/2$ and (b) m_H , as in the corresponding parts of fig. 4.

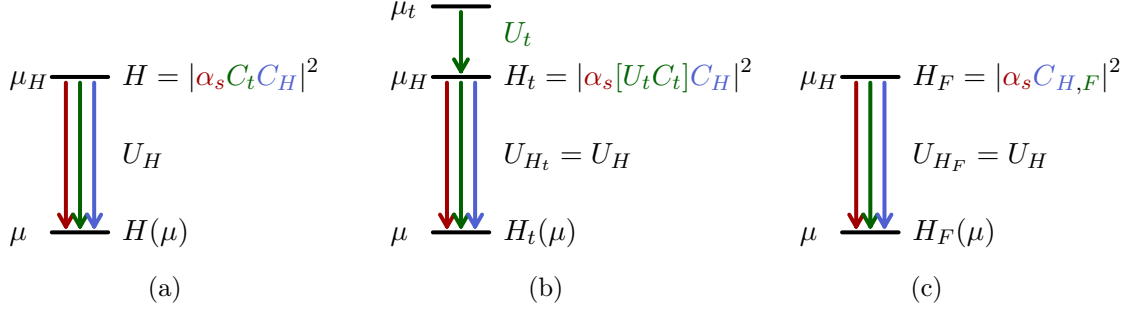


Figure 6: Viable matching schemes for resummation in $gg \rightarrow H$: (a) the effective one-step scheme used in this analysis, (b) two-step matching including U_t -resummation and (c) pure one-step matching with finite top mass terms. While the makeup of H in (a) is discussed in detail in section 2, comparisons to the schemes (b) and (c) can be found in section 4.

results. Since U_H also evolves the overall factor of $|\alpha_s(\mu_H)|^2$ back to the real scale, relative changes of the LO term return the RG evolution of $|C_t \cdot C_H|^2$ along the arc $\mu e^{-i\varphi}$. We observe that this evolution factor varies very little in a neighborhood of $\varphi = \pi/2$, with the maximum precisely coinciding with $\mu_H = -i\mu$ in the case of $\mu = m_H$. Knowing that the final N³LO result is “flat”, this again points at $\mu_H = -i\mu$ being a natural scale of the hard function – by a reversed argument: As the evolution factor attains its maximum, most of the higher order corrections are resummed and collectively become minimal.

4. Comparison of matching schemes

In section 2, we chose to evaluate both C_H and C_t at one single hard scale μ_H . This is not necessarily a natural choice, given our assumption of scale separation between the dynamics of the “top triangle” and the remaining hard virtual corrections: Rather, we should be tempted to evaluate C_t and C_H at the scale intrinsic to each. This is precisely the approach of [6], sketched in fig. 6 (b): By setting up an independent RG evolution U_t for C_t , C_t can be evaluated e.g. at $\mu_t = m_t$ and then RG evolved to μ_H , resumming along the way logarithms L_t, L_t^2 in the expansion (2.6) of C_t . A numerical comparison of this scheme to our results is performed in section 4.1.

There are two main reasons for us to refrain from using the two-step scheme of [6] and to adopt instead the effective one-step scheme in fig. 6 (a): For one, the logarithms $\propto L_t^{n-1}$ at NⁿLO in C_t are not large compared to the Sudakov logarithms $\propto L^{2n}$ in C_H . We therefore focus on resumming the latter under “adverse conditions”: L_t will become numerically larger as $\varphi \rightarrow \pi/2$. On the other hand, these “adverse

conditions” are not arbitrary. An alternative matching scheme exists [7] where the full $n_f = 6$ Standard Model is directly matched onto SCET by means of a single matching coefficient $C_{H,F}$, fig. 6 (c). The obvious advantage is that $C_{H,F}$ will contain the correct dependence on the finite ratio m_t/m_H , currently known through NNLO [15, 16, 17, 18]. The drawback is that logarithms $L_t = \ln(m_t^2/\mu^2)$ still appear in $C_{H,F}$: As the independent running of C_t is lost, there is no way to resum them by RG evolution. These are precisely the conditions under which π^2 -resummation is brought to the test in the present analysis: In section 4.2, we check that our effective one-step scheme (a) is consistent with the finite top mass scheme (c) in the limit of solely logarithmic dependence on the top mass. Since we only intend to resum cross sections computed in the infinite top mass limit [5], our framework will be sufficient. We stress that resummation of more precise results to come will require correct treatment of a finite top mass in the hard function as well. Nonetheless, resummation of the selfsame Sudakov logarithms in $C_{H,F}$ as in C_H will proceed along the steps outlined here and should yield similarly improved convergence of the hard function.

4.1. Two-step matching

The two-step matching scheme in [6] takes into account the independent RG evolution of C_t , driven by its anomalous dimension γ^t . There, an all-orders expression for the evolution factor U_t is given. For comparison, we truncate it at a logarithmic order consistent with the NNLL counting in the main evolution factor U_H . Since C_t has no cusp anomalous dimension and $\gamma_0^t = 0$, the evolution factor simply reads

$$U_t(\mu_t, \mu) = \frac{C_t(m_t^2; \mu)}{C_t(m_t^2; \mu_t)} = \exp [K_{\gamma^t}(\mu_t, \mu)] \stackrel{\text{NNLL}}{=} \exp \left[-\frac{\alpha_s(\mu_t)}{4\pi} \frac{\gamma_1^t}{2\beta_0} (r - 1) \right], \quad (4.1)$$

where $r := \alpha_s(\mu)/\alpha_s(\mu_t)$. On the basis of U_t , we define a modified hard function H_t that internally evolves C_t from μ_t to the hard scale:

$$H_t(m_H^2, m_t^2; \mu_H) = \left| \alpha_s(\mu_H) (C_t(m_t^2; \mu_t) U_t(\mu_t, \mu_H)) C_H(m_H^2; \mu_H) \right|^2. \quad (4.2)$$

Note that the anomalous dimensions of the factors are unchanged. Thus, H_t will still undergo RG evolution by U_H . We now can repeat the numerical calculations of the previous section for H_t . Here, we set $\mu_t = m_t$ in order to eliminate (read: resum) all logarithms $L_t = 0$ from $C_t(\mu_t)$. The absolute values of the fixed order expansions at N³LO vary very little:

$$\begin{aligned} (H_t - H)/H|_{\mu_H=m_H} &= +0.08\% , \\ (H_t - H)/H|_{\mu_H=-im_H} &= -0.17\% \end{aligned} \quad (4.3)$$

We therefore can concentrate on the convergence of H_t . To this end, detail plots are presented in fig. 5 (a) for $\mu = m_H/2$ and in (b) for $\mu = m_H$. Comparing these results to the detail plots in fig. 5, we observe a slightly reduced N³LO correction at $\mu = m_H$. The effect is more pronounced in the case of $\mu = m_H/2$, where both

the NNLO and N³LO corrections are roughly cut down to half. This is as expected, since U_t also resums the real parts of L_t that are enhanced by $2\ln 2$ in the case $\mu = m_H/2$. The results including “internal resummation” also are slightly more stable against variation of the phase around $\varphi = \pi/2$. Yet, both effects are relatively minor, providing evidence that the logarithms L_t are in fact not “large” – even when evaluated in the complex plane at $\mu = -im_H$. It therefore seems safe to forfeit the additional resummation by U_t and the slight benefits it brings to convergence.

4.2. One-step matching with a finite top mass

For pure one-step matching schemes as in fig. 6 (c), the matching coefficient $C_{H,F}$ is known through NNLO. It receives scale-independent contributions $F^{(n)}(m_t, z)$ due to the finite top mass at NⁿLO [7], where $z := m_H^2/(4m_t'^2) < 1$ for the experimentally observed Higgs-like particle. Here, $F^{(2)}$ contains a logarithmic dependence $\propto \ln m_t$. Both $F^{(1)}$ and $F^{(2)}$ contain finite terms $f^{(1,2)}(z) \rightarrow 0$ as $m_t' \rightarrow \infty$.¹² Note that we need to differentiate between the actual top mass m_t , contributing as $\ln m_t$, and a fictitious top mass $m_t' \geq m_t$ that we are free to adjust in order to give a sensible infinite top mass limit to $C_{H,F}$ (and our own hard function $\propto |C_t(\mu_H)|^2$). Additionally, an overall factor of

$$F^{(0)}(z) = \frac{3}{2z} - \frac{3}{2z} \left| 1 - \frac{1}{z} \right| \arcsin^2(\sqrt{z}) \xrightarrow{m_t' \rightarrow \infty} 1 \quad (4.4)$$

encodes the leading order dependence of $C_{H,F}$ on the top mass and enters the hard function $H_F(\mu_H) = |\alpha_s(\mu_H) C_{H,F}(\mu_H)|^2$ as

$$\left| F^{(0)}(z) \right|^2 = 1.065\,02 \text{ for } m_t' = m_t. \quad (4.5)$$

As in section 4.1, the total anomalous dimension of the hard function is unchanged – H_F still undergoes RG evolution by U_H . The authors of [7] worked in the same framework of SCETlib [14] that we used for numerical computations. Conveniently, $f^{(1)}$ was implemented through $\mathcal{O}(z^4)$ in the framework, while $f^{(2)} = f^{(2)}(z=0) + \mathcal{O}(z) = 0$ was kept for simplicity. This allows for a direct numerical comparison between the matching schemes through NNLO. In fig. 7, the fixed order expansions of H and H_F at $\mu_H = m_H$ are compared at NLO and NNLO as a function of $x = m_t/m_t'$. Here, m_t' enters $f^{(1)}$ and the overall factor of $|F^{(0)}|$. By removing the latter from H_F , we compare *normalized* hard functions. The actual value m_t of the top mass is used for the logarithmic terms both in our top matching coefficient C_t and in $F^{(2)}$. A realistic value of m_t' is assumed for $x = 1$ at the right edge of the plot, whereas $x \rightarrow 0$ as $m_t' \rightarrow \infty$ (on the left).

We observe that the deviations between the schemes vanish in the infinite top mass limit $x \rightarrow 0$ as they should. This indicates that our effective one-step scheme becomes in fact equivalent to a proper one-step scheme after reexpanding C_t and

¹²In [7], $F(2)$ is also defined to include all scale-independent terms at NNLO.

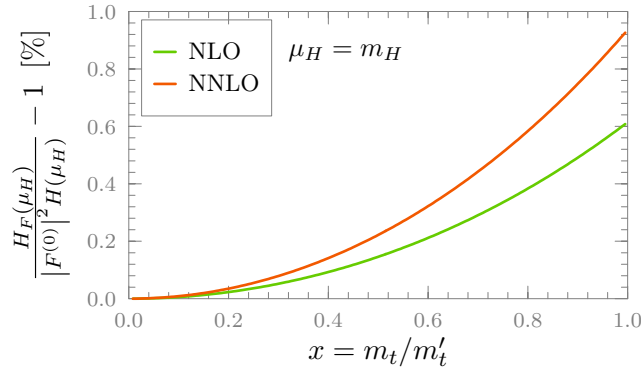


Figure 7: Relative deviation of the pure one-step hard function H_F from the hard function as defined in section 2. Both expansions are truncated at the order indicated by the colors. To compare *normalized* perturbative expansions, the LO top mass dependence $|F^{(0)}|^2$ is removed from H_F . All logarithmic dependencies on the top mass are computed at m_t ; all finite terms in $C_{H,F}$ that are due to a finite top mass are evaluated at $m'_t = m_t/x$. Hence, $x = 1$ corresponds to a realistic setting for the top mass, while $x \rightarrow 0$ as $m'_t \rightarrow \infty$.

C_H against each other.¹³ Yet, fig. 7 also strongly indicates the need to correctly handle finite top mass effects $f^{(1,2)}(z)$ in future resummation of fixed order results. The deviation in the normalized hard function – due to $f^{(1)}$ alone – is at $\approx 1\%$ for the physical value of the top mass $x = 1$, already exceeding typical resummed N³LO corrections brought forth in this analysis (s. fig. 4). On the other hand, the sizable contribution from the LO factor of $F^{(0)}$ is irrelevant for the purpose of resumming cross sections: Here, only *normalized* hard functions enter.

5. π^2 -Resummation of the $gg \rightarrow H$ inclusive cross section

Having analyzed the behavior of the resummed hard function in detail, we now proceed to resum the perturbative series of an actual physical observable – the inclusive $gg \rightarrow H$ cross section. We derive our resummation scheme in section 5.1. In section 5.2, we give a rough overview how the cross section “behaves” under resummation. We then proceed to present our numerical results and improved uncertainty estimates.

5.1. Resummation scheme

To set up our resummation scheme, we resort to a normalized hard function

$$h(\mu) = \frac{H(\mu)}{|\alpha_s(\mu)|^2} \stackrel{\text{fixed order}}{=} 1 + h^{(1)}(\mu) + h^{(2)}(\mu) + \dots \quad (5.1)$$

¹³This equivalence also holds for other choices of the hard scale than the one employed here. For reference, fig. 13 in appendix C contains an analogous plot for $\mu_H = -im_H$.

Its evolution factor is given by

$$U_h(\mu_H, \mu) = \left| \frac{\alpha_s(\mu_H)}{\alpha_s(\mu)} \right|^2 U_H(\mu_H, \mu) = 1 + u^{(1)}(\mu_H, \mu) + u^{(2)}(\mu_H, \mu) + \dots \quad (5.2)$$

in an enhanced expansion in both $\alpha_s(\mu)$ and $\alpha_s(\mu_H)$.¹⁴ For brevity, we omit the arguments of U_h and $u^{(n)}$ in the following. The coefficients of the expansion are fixed by the defining property $h(\mu) = h(\mu_H) U_h(\mu_H, \mu)$ through N³LO as

$$\begin{aligned} u^{(1)} &= h^{(1)}(\mu) - h^{(1)}(\mu_H) , \\ u^{(2)} &= h^{(2)}(\mu) - h^{(2)}(\mu_H) - h^{(1)}(\mu_H) u^{(1)} , \\ u^{(3)} &= h^{(3)}(\mu) - h^{(3)}(\mu_H) - h^{(2)}(\mu_H) u^{(1)} - h^{(1)}(\mu_H) u^{(2)} . \end{aligned} \quad (5.3)$$

Assume we are given the fixed order perturbative series $\sigma_{\text{FO}}(\mu)$ of the inclusive cross section up to some fixed order NⁿLO. It will have a residual dependence on the renormalization scale μ that only vanishes for the all-orders result $n \rightarrow \infty$. We would now like to resum it in a way analogous to the hard function:

$$\begin{aligned} \sigma_{\text{FO}} &= \sigma^{(0)} \left(1 + \tilde{\sigma}_{\text{FO}}^{(1)} + \dots + \tilde{\sigma}_{\text{FO}}^{(n)} \right) , \\ \sigma_{\text{res}} &= U_h \sigma^{(0)} \left(1 + \tilde{\sigma}_{\text{res}}^{(1)} + \dots + \tilde{\sigma}_{\text{res}}^{(n)} \right) \end{aligned} \quad (5.4)$$

To this end, we determine the coefficients $\tilde{\sigma}_{\text{res}}^{(m)}$ for $m \leq n$ by having them satisfy the all-orders condition $\sigma = \sigma_{\text{res}} = \sigma_{\text{FO}}$ at all orders *up to* NⁿLO. This amounts to retroactively “correcting the error” introduced by U_h . Through N³LO, the resulting expressions have the iterative form

$$\begin{aligned} \tilde{\sigma}_{\text{res}}^{(1)} &= \tilde{\sigma}_{\text{FO}}^{(1)} - u^{(1)} , \\ \tilde{\sigma}_{\text{res}}^{(2)} &= \tilde{\sigma}_{\text{FO}}^{(2)} - u^{(2)} - \tilde{\sigma}_{\text{res}}^{(1)} u^{(1)} , \\ \tilde{\sigma}_{\text{res}}^{(3)} &= \tilde{\sigma}_{\text{FO}}^{(3)} - u^{(3)} - \tilde{\sigma}_{\text{res}}^{(2)} u^{(1)} - \tilde{\sigma}_{\text{res}}^{(1)} u^{(2)} . \end{aligned} \quad (5.5)$$

Here, the coefficients $\tilde{\sigma}_{\text{res}}^{(m)}$ inherit the dependence of $\tilde{\sigma}_{\text{FO}}^{(m)}$ on μ . However, they receive an additional dependence on the “internal” hard scale μ_H via the coefficients of U_h . Through this, we will be able to repeat our analysis of suitable phases φ of the hard scale μ_H for the resummed cross section in section 5.2.

However, before we turn to numerical results, we still need to justify our choice of resumming the cross section σ via the RG evolution of the hard function H (or h). The fundamental connection between cross sections and hard functions are *factorization theorems* that can be proven in the framework of SCET. Relevant for our case is the factorization theorem derived in [4]: Consider a central jet veto, imposed by a cut p_{cut} on the transverse momentum $p := p_T^{\text{jet}}$ of final state jets. The

¹⁴Note that removing the running of the overall factor of $|\alpha_s|^2$ from the evolution factor is necessary to write down an expansion $1 + \dots$. In fact, a tiny numerical difference enters here as α_s is run at three-loop in closed form, while it is run by the approximate NNLL expression for K_γ when included in the non-cusp anomalous dimension of C_{ggH} .

cumulant of the cross section up to p_{cut} can then be divided into a singular part (containing IR-poles that cancel against each other) and a non-singular remainder that vanishes linearly as $p_{\text{cut}} \rightarrow 0$. Thus, the total cross section reads

$$\sigma = \sigma_s(p_{\text{cut}}) + \sigma_{\text{ns}}(p_{\text{cut}}) + \int_{p_{\text{cut}}}^{\infty} dp \frac{d\sigma}{dp} . \quad (5.6)$$

Glossing over most of the technicalities,¹⁵ the singular cross section *factorizes* into

$$\sigma_s(p_{\text{cut}}) = \sigma_B \cdot H(\mu) \cdot \int dY B(p_{\text{cut}}, \mu, x_a) \cdot B(p_{\text{cut}}, \mu, x_B) \cdot S(p_{\text{cut}}, \mu) , \quad (5.7)$$

$$x_{a,b} = \frac{m_H}{E_{\text{cm}}} e^{\pm Y} ,$$

where σ_B is the Born cross section, H is the hard function and Y is the pseudo-rapidity of the Higgs. Furthermore, the “beam function” B encodes radiation collinear to the incoming hadrons; B is given by a convolution of regular gluon PDFs and perturbatively accessible matching kernels. Finally, S is a “soft function” representing soft real radiation and is defined as a matrix element of soft Wilson lines.

The connection between the hard function and the non-singular cross section is less clear, on the other hand. Here, only a heuristic argument can be given: As the cut is lifted, $p_{\text{cut}} \rightarrow \infty$, both σ_s and σ_{ns} diverge and the two must cancel to produce a finite total cross section σ . In order for this cancellation to work, $\sigma_{\text{ns}}(p_{\text{cut}} \rightarrow \infty)$ must have a similar makeup as σ_s . We therefore can make the simplified assumption that the fixed order cross section is approximately given by a product,

$$\sigma_{\text{FO}} \approx H(\mu) \cdot R(\mu) = \sigma^{(0)} \left(1 + h^{(1)}(\mu) + \dots \right) \left(1 + r^{(1)}(\mu) + \dots \right) , \quad (5.8)$$

where the scale dependence of H and R has to cancel when $\sigma_{\text{FO}} \rightarrow \sigma$ is evaluated to all orders. In this scenario, it is entirely natural to resum σ_{FO} by means of U_h : Resumming the perturbative series of the first factor leaves just

$$\sigma_{\text{res}} = U_h \sigma^{(0)} \left(1 + h^{(1)}(\mu_H) + \dots \right) \left(1 + r^{(1)}(\mu) + \dots \right) . \quad (5.9)$$

We therefore can expect the resummation by U_h to improve the convergence of σ , as well, if we chose μ_H such as to minimize the perturbative corrections $h^{(m)}(\mu_H)$. Note that the resummation may still lead to naught, if a large cancellation between $h^{(m)}$ and $r^{(m)}$ (and their cross terms) “secretly” occurs in the expansion of σ_{FO} .

5.2. Numerical results and uncertainties

On the grounds of the resummation scheme (5.3), (5.4), (5.5) presented in the previous section, we now give numerical results for the resummed cross section after a rough overview of its behavior. We use the fixed order results for the inclusive cross

¹⁵And the fact that beam and soft functions will depend on another “rapidity scale” ν .

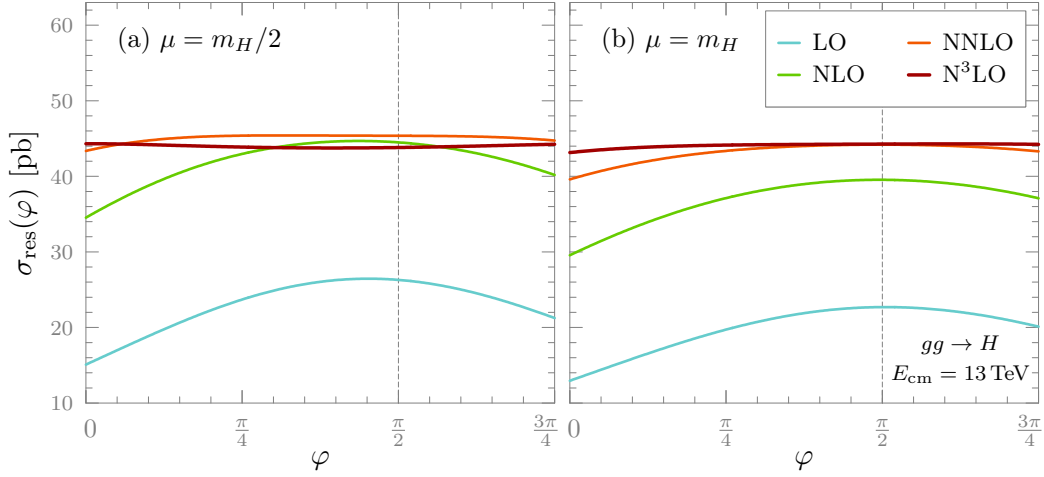


Figure 8: The resummed inclusive cross section σ_{res} in (5.4) for different values of φ , $\mu_H = \mu e^{-i\varphi}$. As above, colors indicate the order at which σ_{res} is truncated; darker colors correspond to higher orders.

section at a renormalization and factorization scale $\mu = m_H/4, m_H/2, m_H, 2m_H$ obtained in [5].¹⁶ Since they assume an infinitely heavy top quark (and consequently omit the leading order factor of $|F^{(0)}|^2$ in the cross-section, too), our framework of effective one-step matching is sufficient to attempt a resummation. Like the original results, our results are valid for a hadronic $E_{\text{cm}} = 13 \text{ TeV}$. Figure 8 shows the resummed cross section at different values of the phase φ of the internal resummation scale μ_H . Here, the evolution factor U_h in (5.4) is evaluated at NNLL precision throughout. The resummed series of σ_{res} is truncated at the order indicated by the colors. At $\varphi = 0$, the original fixed order results are reproduced as $U_h = 1$.

Key observations made on the resummed hard function in section 3 are reproduced here for the cross section: Again, the convergence of the perturbative series is markedly improved by the resummation around $\varphi \approx \pi/2$: The improvement is entirely unambiguous in the case of $\mu = m_H$ in fig. 8 (b), leaving the N^3LO correction almost obsolete. For $\mu = m_H/2$, the NNLO correction decreases strongly as $\varphi \approx \pi/2$, making the coveted smallness of the N^3LO correction at $\varphi = 0$ appear rather accidental. The N^3LO results apparently inherit their stability under variations of φ from the hard function. More generally speaking, there is a close similarity in behavior to the hard function when undergoing resummation. This is compelling evidence that the large logarithms in the hard function are the same that obstruct the convergence of σ_{FO} . Put differently, it indicates that the cross section contains no “secret cancellation” between said logarithms and competing terms.

By means of our resummation scheme, improved and more reliable estimates for

¹⁶Unfortunately, genuine numerical values could not be retrieved from the authors of [5] for lack of time. We therefore have to rely on numerical values extracted from their fig. 2 for all scales and orders except for $\mu = m_H/2$ and m_H at N^3LO . (For these, numerical values are given in tabular form.)

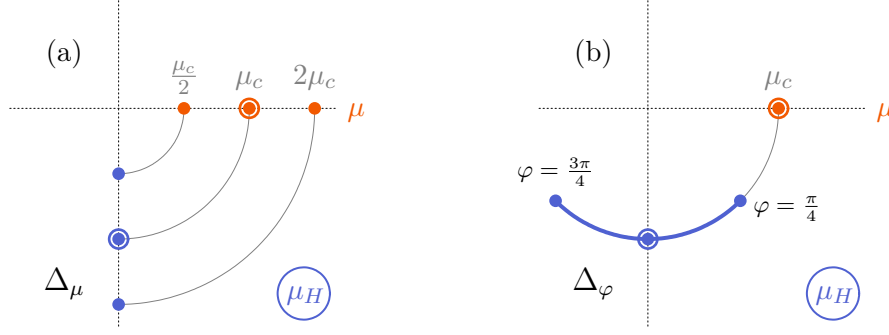


Figure 9: Variation schemes used to estimate uncertainties. In (a), the phase of the hard scale is fixed at $\varphi = \pi/2$, $\mu_H = -i\mu$, while μ is varied by a factor of 2 from a central scale μ_c to estimate Δ_μ . In (b), $|\mu_H| = \mu_c$ is fixed, but a scan in φ over $[\pi/4, 3\pi/4]$, $\mu_H = \mu_c e^{-i\varphi}$, is performed to estimate Δ_φ . A possible path of the RG evolution used for resummation is indicated in grey.

the perturbative uncertainties of σ can also be obtained. To arrive at this core result of our analysis, we first define the relevant uncertainties and then give detailed numerical results. Consider the resummed cross section σ_{res} for the most relevant choice of the hard scale, $\varphi = \pi/2$, $\mu_H = -i\mu$. Two independent sources of uncertainty can be made out for σ_{res} : First, the all-orders result for the cross-section has to be independent of the renormalization scale μ . The residual dependence on μ therefore is an indicator of how reliable the perturbative result already is. For a given central scale μ_c , we estimate this uncertainty Δ_μ by setting $\mu = \mu_c/2$ and $\mu = 2\mu_c$ and computing the maximum deviation from the value of σ_{res} at μ_c . The resummation scale μ_H is kept at $\mu_H = -i\mu$ throughout, i.e. varied simultaneously with μ . Figure 9 (a) shows a sketch of the variation scheme. When applied to the original fixed order results at $\varphi = 0$, Δ_μ will reproduce the maximum of the upper and lower uncertainties given in [5].¹⁷

Second, we also take into account possible uncertainties due to the additional scale μ_H we introduce. Uncertainties due to $|\mu_H|$ are already covered by the simultaneous variation in Δ_μ . To estimate the uncertainty Δ_φ induced by φ for a given central scale μ_c , we let the hard scale μ_H sweep the arc $\mu_c e^{-i\varphi}$, $\varphi \in [\pi/4, 3\pi/4]$ as in fig. 9 (b) and compute the maximum deviation from σ_{res} at $\varphi = \pi/2$ along the entire arc. An estimate of the total uncertainty Δ of σ_{res} is then obtained as

$$\Delta^2 = \Delta_\varphi^2 + \Delta_\mu^2. \quad (5.10)$$

Figure 10 shows our results for the resummed cross section at $\mu = m_H/2$ and $\mu = m_H$ in direct comparison to the original results from [5]. Uncertainties for the fixed order results (on the left) essentially are maximal symmetric uncertainties from

¹⁷In [5], the uncertainties are estimated by a full scan over the interval $\mu \in [\mu_c/2, 2\mu_c]$. However, one of the boundaries of the interval is almost sure to coincide with the maximum deviation.

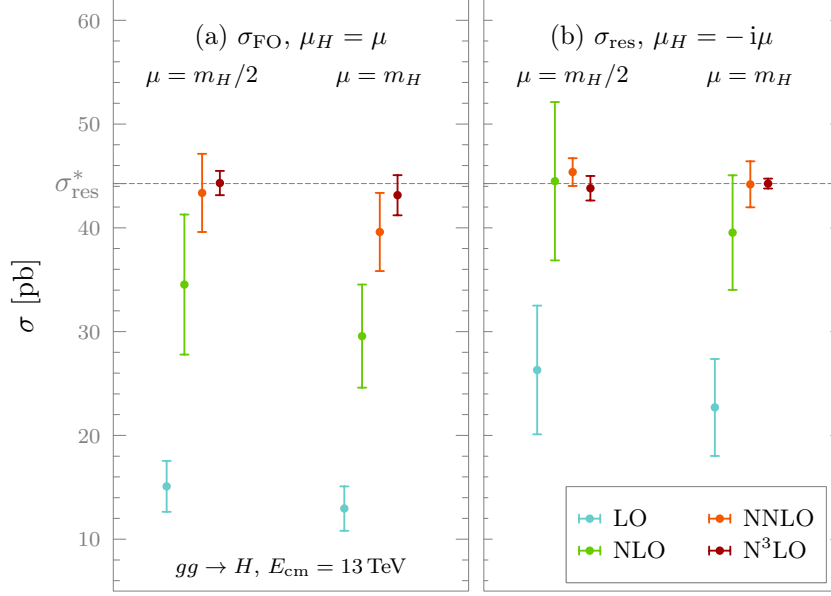


Figure 10: Results for the inclusive cross section. Shown in (a) are the original fixed order results [5] with maximal symmetric uncertainties; (b) shows our resummed results with uncertainty estimates as in (5.10). As usual, darker colors correspond to higher orders in the perturbative series. The dashed line indicates our best resummed N³LO estimate σ_{res}^* at $\mu = m_H$.

the original reference. The uncertainties Δ for our results (right) are computed as outlined above. They are broken down into the contributions from Δ_μ and Δ_φ in table 3 and table 4, respectively. Table 2 in appendix C contains the numerical values for fig. 10, presenting relative uncertainties.

We can waive pointing out the improved convergence (already discussed above) and focus immediately on the uncertainties, in particular on those of the π^2 -resummed results at $\mu = m_H$. Here, both the NLO and NNLO uncertainty estimates contain all higher order results, giving evidence that they reasonably cover the uncertainty from missing higher order. This overlap is present in the original fixed order results only at NNLO, with similar sizes of the uncertainties. While it can also be observed for the resummed result at $\mu = m_H/2$, it comes at the cost of higher uncertainties. It is remarkable that the resummed N³LO result at $\mu = m_H$ can be estimated down to a very narrow band of $\pm 1.1\%$, demonstrating all over again that $\mu_H = -im_H$ is in fact a natural choice of scale. Yet, this narrow band still contains the resummed result at $\mu = m_H/2$ and the best original estimate at the scale $\mu = m_H/2$ favored by the authors.

This sizable reduction in uncertainty at N³LO can to a great extent be attributed to a reduced uncertainty from μ . This can be observed directly in fig. 10, where the resummed values at N³LO differ slightly less from each other than the original results. On the other hand, uncertainties from φ are substantially smaller than the ones originating in variation of μ at N³LO. Polemics could also claim that the NNLO

result σ_{res} at $\mu = m_H$ already matched the best N³LO estimate, making it a futile task to implement the hard function through N³LO. We now see that this is not quite true: At lower orders, Δ_φ becomes sizable and contributes roughly as much as Δ_μ (table 3, table 4). Thus, the improved estimate for the N³LO uncertainty at $\mu = m_H$ is at least in part owed to the fact that only at N³LO, the hard function becomes sufficiently stable under variation of φ .

6. Outlook on the N³LO Drell-Yan hard function

As another process where a color singlet is produced, we can consider the Drell-Yan case. The hard function in this case only consists of one single Wilson coefficient C_H matching full QCD on SCET,

$$H_{\text{DY}}(Q^2; \mu) = |C_H(Q^2; \mu)|^2, \quad (6.1)$$

where $Q^2 = q^2$ is the invariant mass of the intermediate photon or Z boson. The calculation of C_H at NLO has been sketched in section 1.2. At N³LO, it can be obtained in a way similar to the $gg \rightarrow H$ hard matching coefficient from the quark (instead of the gluon) form factor in QCD. Again, IR-poles in the form factor are reinterpreted as UV-divergencies of SCET and removed by a multiplicative renormalization. The IR-finite terms of the form factor yield the boundary condition of the resulting RGE:

$$\mu \frac{d}{d\mu} C_H = \left[\Gamma^F(\alpha_s) \ln \frac{-m_H^2 - i0}{\mu^2} + \gamma^{\text{DY}} \right] C_H, \quad (6.2)$$

where $\Gamma^F = (C_F/C_A) \cdot \Gamma^A$ due to Casimir scaling at all orders known so far.¹⁸

To implement the perturbative series, we make good use of the generic expression (B.5) derived in appendix B:

$$C_H(Q^2; \mu) = 1 + \sum_{n=1}^{\infty} \left(\frac{\alpha_s(\mu)}{4\pi} \right)^n C_H^{(n)}(L), \quad L := \ln \frac{-Q^2 - i0}{\mu^2} \quad (6.3)$$

Here, the boundary conditions $d_H^{(n)}$ at $L = 0$ were again read off from the results in [11]. At N³LO, i.e. in $d_H^{(3)}$, the authors of [11] also include a contribution $\propto N_{F,V}$ from diagrams without direct coupling of the intermediate boson to the initial state quarks $q\bar{q}$. However, we choose to omit the term, since in the same reference a full expression for $N_{F,V}$ is only provided assuming purely electromagnetic interaction. (As contributions from an on-shell Z will be dominant, this assumption can not be valid.) When evaluated for $q = u$ (d) the purely electromagnetic contribution is -2.97 (5.94) compared to a numerical value of $d_H^{(3)} = -1386.71$ and would in fact be negligible when entering the hard function with a factor of $2 \text{Re}(\alpha_s/4\pi)^3$ in front.

¹⁸Sources cited for the anomalous dimensions are compiled in appendix A.

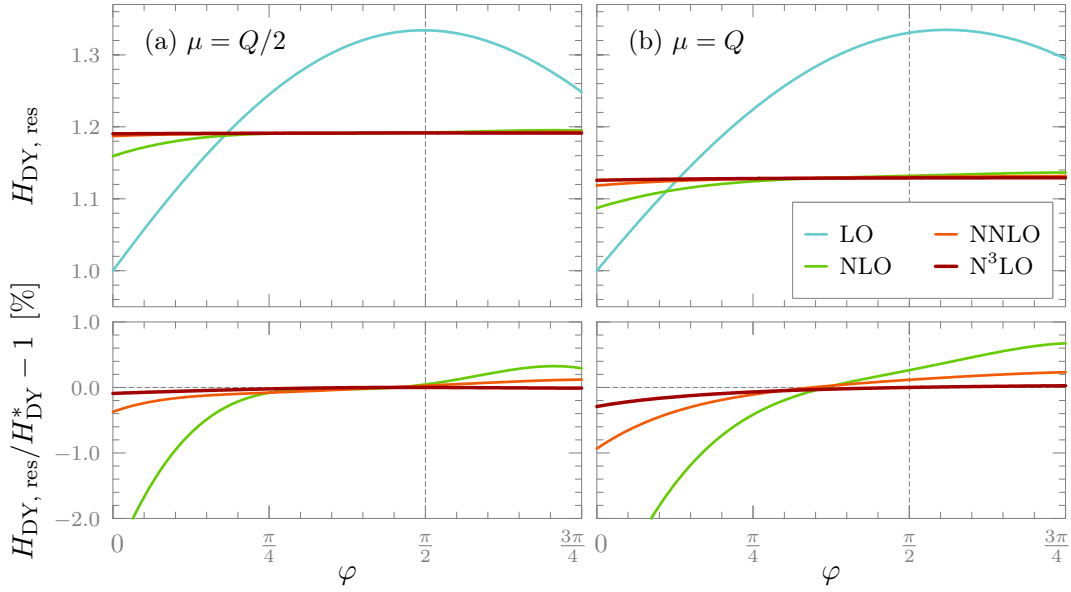


Figure 11: The RG evolved hard function H_{res} for the Drell-Yan case as a function of φ , $\mu_H = \mu e^{-i\varphi}$, where (a) $\mu = Q/2$ on the left and (b) $\mu = Q$ on the right. Colors correspond to the fixed order truncation. The bottom row (detail) again shows the relative deviation from the $N^3\text{LO}$ value H_{DY}^* at $\varphi = \pi/2$.

Note that we normalize the LO contribution in (6.3) to 1. We correspondingly do not include overall factors that would account for the electro-weak coupling of the incoming quarks or the Z propagator. For this reason, C_H and H_{DY} only depend on the ratio μ/Q . We note in passing that when restricted to $\mu \in \mathbb{R}$ and expressed in terms of $L_Q := \ln(\mu/Q)$, $L = i\pi - 2L_Q$, our result for the $N^3\text{LO}$ hard function is in perfect numerical agreement with [19], corroborating the validity of the generic expression (B.5).

In a manner completely analogous to the $gg \rightarrow H$ hard function, H_{DY} can be evaluated at a scale μ_H in the complex plane and then RG evolved back to a real-valued scale μ . For our numerical results, we again vary the phase of μ_H as $\mu_H = \mu e^{-i\varphi}$. The results of the procedure are shown in fig. 11 (a) for $\mu = Q/2$ and in (b) for $\mu = Q$; the evolution factor is evaluated at NNLL precision. We observe that while the convergence of the perturbative series at $\varphi = \pi/2$ is slightly improved by resummation for both cases, the effect is nowhere near the vast effect observed for gluon fusion. In particular, the series converges remarkably well even before resummation, with $N^3\text{LO}$ corrections amounting to less than 1 %. Numerical values of the normalized hard function to illustrate this further are

$$\begin{aligned} H_{\text{DY}}/H_{\text{DY,LO}}|_{\mu_H=Q} &= 1 + 0.08726 + 0.03115 + 0.00726, \\ H_{\text{DY}}/H_{\text{DY,LO}}|_{\mu_H=-iQ} &= 1 - 0.14935 - 0.00125 - 0.00099 \end{aligned} \quad (6.4)$$

As noted in [3], this is mostly due to the numerically smaller cusp anomalous dimension in the Drell-Yan case, $\Gamma_F/\Gamma_A = C_F/C_A = 4/9$. Hence, the leading π^2 -enhanced

terms L^{2n} at N³LO in the fixed order expansion at a real-valued scale are also suppressed by $(4/9)^n$, leaving less room for improvement of the convergence by resummation. Furthermore, we remark that the choice $\mu_H = -iQ$, $L = 0$ is not as clearly superior to $\mu_H = -iQ/2$ as in the gluon fusion case. In fact, the convergence of H_{DY} at the latter scale even is slightly better, further indicating that C_H is not entirely dominated by the Sudakov logarithms L^{2n} . Rather, the additional real part of $2 \ln 2$ seems to move L closer to a “compromise” between the roots of $C_H^{(n)}$.

7. Conclusions

We have extended the hard function for gluon fusion Higgs production to N³LO in an effective one-step matching scheme. Evaluating the hard function at an additional scale μ_H and subsequently RG evolving it at NNLL, we have been able to resum its perturbative series. After direct comparison between different values for $\varphi = -\arg \mu_H$, our results strongly suggest the prescription $\mu_H = -im_H$ of π^2 -resummation as a natural scale for the hard function: By this choice, the convergence of its perturbative series is vastly improved, as leading Sudakov logarithms will be resummed completely. The benefits of two-step matching schemes [6] have been found to be minor. On the other hand, we expect finite top mass effects from pure one-step matching [7] to become relevant in further analyses. Through NNLO, we have demonstrated that our matching scheme reproduces the infinite top mass limit of pure one-step matching.

By applying the same resummation scheme to the total cross section for gluon fusion at fixed order N³LO [5], we have demonstrated that here as well, π^2 -resummation at $\mu_H = -im_H$ will yield the fastest convergence of the perturbative series. By varying both φ and the renormalization and factorization scale μ , we have arrived at improved estimates for the perturbative uncertainties of the cross section. Our best estimate for the N³LO total cross section for gluon fusion at $E_{\text{cm}} = 13 \text{ TeV}$ is

$$\sigma_{gg \rightarrow H} = 44.27 \text{ pb} \pm_{\mu} 1.03 \% \pm_{\varphi} 0.31 \% = 44.27 \text{ pb} \pm 1.08 \% .$$

To further improve this estimate, we endorse extending the evolution factor to N³LL as soon as the necessary four-loop cusp anomalous dimension becomes available. Accounting for the uncertainties of α_s in a more elaborate variation scheme may also be in order.

In the case of the Drell-Yan process, we observe a slightly improved convergence of the hard function after π^2 -resummation at N³LO. The effect is much less pronounced than in the gluon fusion case, as was observed at lower orders before [3]. Whether the slight improvement carries through to cross sections and rapidity spectra could be subject to further investigation.

A. Anomalous dimensions

The β -function of QCD is expanded as

$$\mu \frac{d\alpha_s}{d\mu} = \beta(\alpha_s) = -2\alpha_s \sum_{n=0}^{\infty} \beta_n \left(\frac{\alpha_s}{4\pi} \right)^{n+1}. \quad (\text{A.1})$$

All cusp and non-cusp anomalous dimensions throughout the text are expanded as

$$\gamma(\alpha_s) = \sum_{n=0}^{\infty} \gamma_n \left(\frac{\alpha_s}{4\pi} \right)^{n+1}, \quad \Gamma(\alpha_s) = \sum_{n=0}^{\infty} \Gamma_n \left(\frac{\alpha_s}{4\pi} \right)^{n+1}. \quad (\text{A.2})$$

Sources cited for particular coefficients are compiled in table 1 below.

β_n	consistent with	[7], [11]	
γ_n^t	cited from	[6]	
γ_n^H	cited from	[6]	given there as γ_n^S
$\Gamma_n^{A,F}$	cited from	[7]	given there as $\Gamma_n^{g,q}$
	consistent with	[11]	given there as $\gamma_n^{\text{cusp}} \cdot C^{A,F}$
γ_n^{ggH}	by (2.10) consistent with	[7]	given there as γ_{Hn}^g
	by (2.10) consistent with	[11]	given there as $\textcolor{red}{2}\gamma_n^g$
γ_n^{DY}	cited from	[11]	given there as $\textcolor{red}{2}\gamma_n^q$

Table 1: Sources cited and cross-checked for the coefficients of various anomalous dimensions. For definitions of the anomalous dimensions, see the text. All consistency checks have been performed up to 3-loop ($n = 0, 1, 2$). The factor of $\textcolor{red}{2}$ in the Drell-Yan case is checked implicitly by comparing the hard function constructed from γ^{DY} against [19].

B. Generic fixed order expansion of matching coefficients

Consider a matching coefficient C satisfying a generic RGE

$$\mu \frac{d}{d\mu} C(\mu) = [\Gamma(\alpha_s(\mu)) \cdot L + \gamma(\alpha_s(\mu))] C(\mu), \quad (\text{B.1})$$

where Γ and γ are its cusp and non-cusp anomalous dimensions, respectively, and $L = \ln(M^2/\mu^2)$ is a logarithm of the renormalization scale μ and some characteristic mass scale M .¹⁹ The coefficients $C^{(n)}$ in the fixed order expansion

$$C = \sum_{n=0}^{\infty} \left(\frac{\alpha_s(\mu)}{4\pi} \right)^n C^{(n)} \quad (\text{B.2})$$

¹⁹Note that an imaginary-valued $M = -iQ$ as for the SCET hard matching coefficients C_H in both Higgs production and the Drell-Yan case does not affect the derivation presented here. In these cases, a prescription of $(-i)^2 = -1 - i0$ is understood.

then satisfy a set of coupled differential equations: Expanding the left hand side of (B.1) in powers of $\alpha_s = \alpha_s(\mu)$ leads to

$$\begin{aligned} \text{l. h. s.} &= \sum_{n=0}^{\infty} \left(\frac{\alpha_s}{4\pi} \right)^n \mu \frac{d}{d\mu} C^{(n)} - 2 \sum_{n=1}^{\infty} n \sum_{m=0}^{\infty} \beta_m \left(\frac{\alpha_s}{4\pi} \right)^{n+m+1} C^{(n)} \\ &= \sum_{n=0}^{\infty} \left(\frac{\alpha_s}{4\pi} \right)^n \mu \frac{d}{d\mu} C^{(n)} - 2 \sum_{n=2}^{\infty} \left(\frac{\alpha_s}{4\pi} \right)^n \sum_{m=1}^{n-1} m \beta_{n-m-1} C^{(m)} \end{aligned}$$

after inserting $\mu(d\alpha_s/d\mu) = \beta(\alpha_s)$ as expanded in (A.1) and a simple index shift. On the other hand, expanding the right hand side leaves

$$\text{r. h. s.} = \sum_{n=1}^{\infty} \left(\frac{\alpha_s}{4\pi} \right)^n \sum_{m=0}^{n-1} [\Gamma_{n-m-1} \cdot L + \gamma_{n-m-1}] C^{(m)} .$$

Comparing the two expansions order by order results in

$$\begin{aligned} \mu \frac{d}{d\mu} C^{(0)} &= 0 , \\ \mu \frac{d}{d\mu} C^{(n)} &= \sum_{m=0}^{n-1} [\Gamma_{n-m-1} \cdot L + \gamma_{n-m-1} + 2m\beta_{n-m-1}] C^{(m)} , \quad n > 0 . \end{aligned} \quad (\text{B.3})$$

Let now $d^{(n)}$ be the expansion coefficients of C at $L = 0$,

$$C|_{L=0} = \sum_{n=0}^{\infty} \left(\frac{\alpha_s(\mu)}{4\pi} \right)^n d^{(n)} . \quad (\text{B.4})$$

Setting $d^{(0)} = 1$ for simplicity and recalling $\mu(d/d\mu) = -2d/dL$, (B.3) can be integrated iteratively to obtain the full scale dependence of C . Through N³LO, the resulting polynomials in L require the three-loop coefficients of γ and Γ (as well as $d^{(n)}$ up to N³LO, of course) and read

$$\begin{aligned} C^{(0)} &= 1 , \\ C^{(1)} &= d^{(1)} - \frac{L}{2} \gamma_0 - \frac{L^2}{4} \Gamma_0 , \\ C^{(2)} &= d^{(2)} + \frac{L}{2} \left(-2d^{(1)}\beta_0 - d^{(1)}\gamma_0 - \gamma_1 \right) \\ &\quad + \frac{L^2}{8} \left(2\beta_0\gamma_0 + \gamma_0^2 - 2d^{(1)}\Gamma_0 - 2\Gamma_1 \right) \\ &\quad + \frac{L^3}{24} \Gamma_0 (2\beta_0 + 3\gamma_0) + \frac{L^4}{32} \Gamma_0^2 , \\ C^{(3)} &= d^{(3)} + \frac{L}{2} \left(-4d^{(2)}\beta_0 - 2d^{(1)}\beta_1 - d^{(2)}\gamma_0 - d^{(1)}\gamma_1 - \gamma_2 \right) \\ &\quad + \frac{L^2}{8} \left(8d^{(1)}\beta_0^2 + 6d^{(1)}\beta_0\gamma_0 + 2\beta_1\gamma_0 + d^{(1)}\gamma_0^2 + 4\beta_0\gamma_1 \right. \\ &\quad \left. + 2\gamma_0\gamma_1 - 2d^{(2)}\Gamma_0 - 2d^{(1)}\Gamma_1 - 2\Gamma_2 \right) \end{aligned}$$

$$\begin{aligned}
 & + \frac{L^3}{48} \left(-8\beta_0^2\gamma_0 - 6\beta_0\gamma_0^2 - \gamma_0^3 + 16d^{(1)}\beta_0\Gamma_0 + 4\beta_1\Gamma_0 \right. \\
 & \quad \left. + 6d^{(1)}\gamma_0\Gamma_0 + 6\gamma_1\Gamma_0 + 8\beta_0\Gamma_1 + 6\gamma_0\Gamma_1 \right) \\
 & + \frac{L^4}{96} \Gamma_0 \left(-4\beta_0^2 - 10\beta_0\gamma_0 - 3\gamma_0^2 + 3d^{(1)}\Gamma_0 + 6\Gamma_1 \right) \\
 & + \frac{L^5}{192} \Gamma_0^2 (-4\beta_0 - 3\gamma_0) - \frac{L^6}{384} \Gamma_0^3. \tag{B.5}
 \end{aligned}$$

Note that $d^{(0)} \neq 1$ can easily be taken care of: At each order, $C^{(n)}$ is the integral of lower order coefficients with a boundary condition linear in $d^{(n)}$. By induction, $(d^{(0)}, \dots, d^{(n)}) \mapsto C^{(n)}$ is a linear map onto the polynomials in L at any order. Accounting for $d^{(0)} \neq 1$ just amounts to inserting $d^{(0)}$ in all terms of (B.5) that do not yet contain $d^{(1)}, d^{(2)}, d^{(3)}$, thereby restoring linearity.

C. Further numerical results

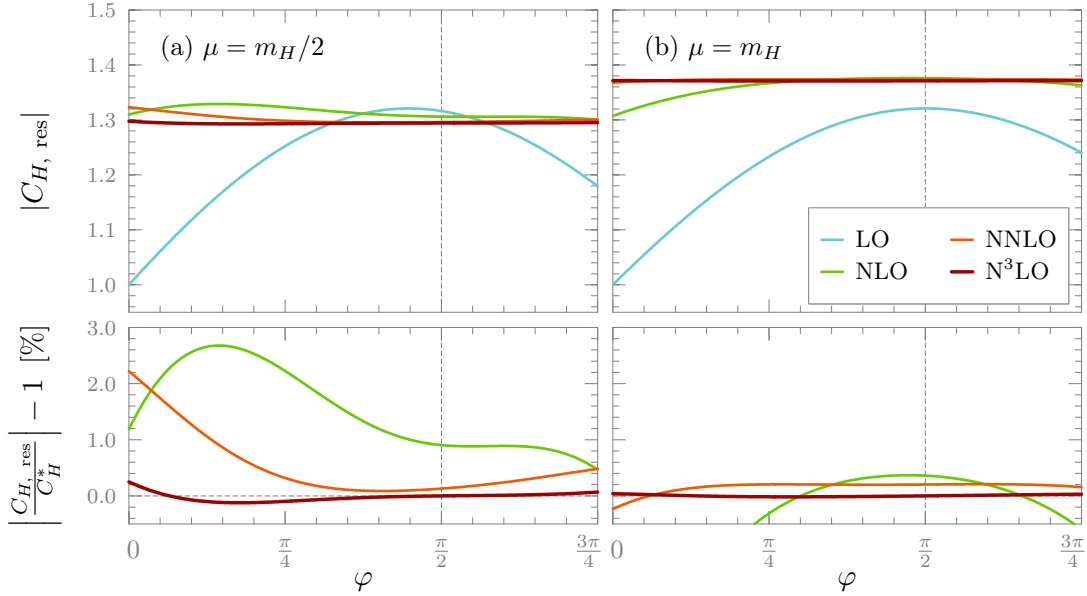


Figure 12: Numerical results for the RG evolved matching coefficient $C_{H,\text{res}} = C_H(\mu_H) U_C(\mu_H, \mu)$ as a function of φ , $\mu_H = \mu e^{-i\varphi}$. As usual, colors indicate the order at which $C_H(\mu_H)$ is truncated; darker colors correspond to higher orders. The evolution factor U_C of C_H is obtained from its RGE (2.8) by means of the helper functions η_Γ , K_Γ , K_γ (2.12) and evaluated at NNLL precision. The top row contains absolute values: The difference in the N³LO result between the cases (a) and (b) is due to RG evolution *along* the real axis. The bottom row displays the relative deviation from the N³LO value C_H^* at $\varphi = \pi/2$.

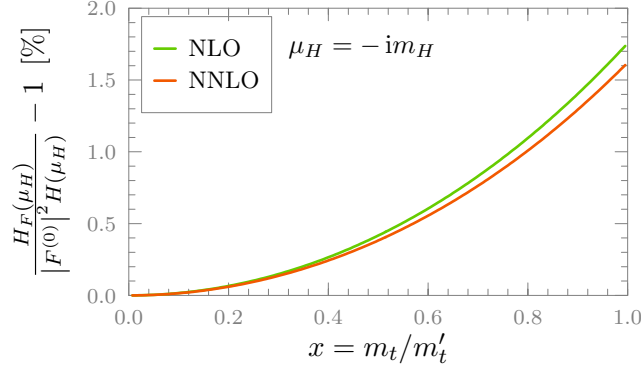


Figure 13: Relative deviation of the pure one-step hard function H_F (section 4.2) from our hard function as defined in section 2. Here, $x \rightarrow 0$, $m'_t \rightarrow \infty$ corresponds to the infinite top mass limit where the two hard functions should coincide. The factor of $|F^{(0)}|^2$ is removed from H_F to compare normalized hard functions. The plot above is completely analogous to fig. 7. The only difference is the choice of $\mu_H = -im_H$ to evaluate the hard functions (instead of $\mu_H = m_H$ in fig. 7.)

σ [pb]	μ	LO	NLO	NNLO	N ³ LO
σ_{FO}	$m_H/2$	15.09 \pm 16.24 %	34.53 \pm 19.53 %	43.36 \pm 8.69 %	44.31 \pm 2.64 %
σ_{FO}	m_H	12.95 \pm 16.50 %	29.56 \pm 16.80 %	39.59 \pm 9.51 %	43.14 \pm 4.47 %
σ_{res}	$m_H/2$	26.30 \pm 23.58 %	44.49 \pm 17.15 %	45.37 \pm 2.95 %	43.81 \pm 2.69 %
σ_{res}	m_H	22.70 \pm 20.59 %	39.54 \pm 14.96 %	44.19 \pm 5.01 %	44.27 \pm 1.08 %

Table 2: Numerical values and relative uncertainties for the inclusive $gg \rightarrow H$ cross sections in fig. 10. The two top rows contain the original values for the fixed order cross sections from [5], where μ is both the factorization and renormalization scale. The bottom rows show our resummed results, where the uncertainties are estimated by contributions from varying both μ and φ according to (5.10).

Δ_μ (rel.)	LO	NLO	NNLO	N ³ LO
$\mu = m_H/2$	13.69 %	14.15 %	2.59 %	2.51 %
$\mu = m_H$	15.87 %	12.52 %	4.59 %	1.03 %

Table 3: Contributions Δ_μ to the relative uncertainty of the resummed cross section. For this estimate, we vary μ by factors of 2 and compute the maximum deviation. The variation scheme is described in section 5.2 and drawn in fig. 9 (a).

Δ_φ (rel.)	LO	NLO	NNLO	N ³ LO
$\mu = m_H/2$	19.20 %	9.70 %	1.40 %	0.98 %
$\mu = m_H$	13.12 %	6.17 %	2.02 %	0.31 %

Table 4: Contributions Δ_φ to the relative uncertainty of the resummed cross section. Here, we vary φ along the arc $[\pi/4, 3\pi/4]$ and compute the maximum deviation. The variation scheme is drawn in fig. 9 (b).

References

- [1] G. Aad et al., ATLAS Collaboration. “Observation of a new particle in the search for the Standard Model Higgs boson with the ATLAS detector at the LHC.” *Phys. Lett. B* 716 (2012), pp. 1–29. arXiv: [1207.7214 \[hep-ex\]](#).
- [2] S. Chatrchyan et al., CMS Collaboration. “Observation of a new boson at a mass of 125 GeV with the CMS experiment at the LHC.” *Phys. Lett. B* 716 (2012), pp. 30–61. arXiv: [1207.7235 \[hep-ex\]](#).
- [3] V. Ahrens, T. Becher, M. Neubert, and L. L. Yang. “Origin of the large perturbative corrections to Higgs production at hadron colliders.” *Physical Review D* 79 (3 2009). arXiv: [0808.3008 \[hep-ph\]](#).
- [4] I. W. Stewart, F. J. Tackmann, J. R. Walsh, and S. Zuberi. “Jet p_T resummation in Higgs production at NNLL’ + NNLO.” *Physical Review D* 89 (5 2014). arXiv: [1307.1808 \[hep-ph\]](#).
- [5] C. Anastasiou, C. Duhr, F. Dulat, F. Herzog, and B. Mistlberger. “Higgs Boson Gluon-Fusion Production in QCD at Three Loops.” *Physical Review Letters* 114 (21 2015). arXiv: [1503.06056 \[hep-ph\]](#).
- [6] V. Ahrens, T. Becher, M. Neubert, and L. L. Yang. “Renormalization-group improved prediction for Higgs production at hadron colliders.” *The European Physical Journal C* 62 (2 2009), pp. 333–353. arXiv: [0809.4283 \[hep-ph\]](#).
- [7] C. F. Berger, C. Marcantonini, I. W. Stewart, F. J. Tackmann, and W. J. Waalewijn. “Higgs production with a central jet veto at NNLL+NNLO.” *Journal of High Energy Physics* 2011 (4 2011). arXiv: [1012.4480 \[hep-ph\]](#).
- [8] I. W. Stewart. *Effective Field Theory. Lecture Notes*. Massachusetts Institute of Technology, 2014. URL: https://courses.edx.org/c4x/MITx/8.EFTx/asset/notes_EFT.pdf.
- [9] I. W. Stewart. *Lectures on the Soft-Collinear Effective Theory*. Massachusetts Institute of Technology, 2013. URL: <http://ocw.mit.edu/courses/physics/8-851-effective-field-theory-spring-2013>.
- [10] C. W. Bauer, S. Fleming, D. Pirjol, and I. W. Stewart. “An effective field theory for collinear and soft gluons: Heavy to light decays.” *Physical Review D* 63 (11 2001). arXiv: [hep-ph/0011336](#).
- [11] T. Gehrmann, Glover, E. W. N., T. Huber, N. Ikizlerli, and C. Studerus. “Calculation of the quark and gluon form factors to three loops in QCD.” *Journal of High Energy Physics* 2010 (6 2010). arXiv: [1004.3653 \[hep-ph\]](#).
- [12] Y. Schröder and M. Steinhauser. “Four-loop decoupling relations for the strong coupling.” *Journal of High Energy Physics* 2006 (01 2006), p. 51. arXiv: [hep-ph/0512058](#).
- [13] K. G. Chetyrkin, J. H. Kühn, and C. Sturm. “QCD decoupling at four loops.” *Nuclear Physics B* 744 (1-2 2006), pp. 121–135. arXiv: [hep-ph/0512060](#).

- [14] F. Tackmann et al. *SCETlib – A C++ package for numerical computations in QCD SCET*. 2015 (under construction, not yet public). URL: <https://confluence.desy.de/display/scetlib>.
- [15] R. V. Harlander and P. Kant. “Higgs production and decay: analytic results at next-to-leading order QCD.” *Journal of High Energy Physics* 2005 (12 2005), p. 15. arXiv: [hep-ph/0509189](https://arxiv.org/abs/hep-ph/0509189).
- [16] C. Anastasiou, S. Beerli, S. Bucherer, A. Daleo, and Z. Kunszt. “Two-loop amplitudes and master integrals for the production of a Higgs boson via a massive quark and a scalar-quark loop.” *Journal of High Energy Physics* 2007 (01 2007), p. 82. arXiv: [hep-ph/0611236](https://arxiv.org/abs/hep-ph/0611236).
- [17] R. V. Harlander and K. J. Ozeren. “Top mass effects in Higgs production at next-to-next-to-leading order QCD: Virtual corrections.” *Physics Letters B* 679 (5 2009), pp. 467–472. arXiv: [0907.2997](https://arxiv.org/abs/0907.2997) [[hep-ph](#)].
- [18] A. Pak, M. Rogal, and M. Steinhauser. “Virtual three-loop corrections to Higgs boson production in gluon fusion for finite top quark mass.” *Physics Letters B* 679 (5 2009), pp. 473–477. arXiv: [0907.2998](https://arxiv.org/abs/0907.2998) [[hep-ph](#)].
- [19] R. Abbate, M. Fickinger, A. H. Hoang, V. Mateu, and I. W. Stewart. “Thrust at N3LL with power corrections and a precision global fit for $\alpha_s(m_Z)$.” *Physical Review D* 83 (7 2011). arXiv: [1006.3080](https://arxiv.org/abs/1006.3080) [[hep-ph](#)].